Computers and Geotechnics 65 (2015) 250–257

Contents lists available at ScienceDirect

Computers and Geotechnics

journal homepage: www.elsevier.com/locate/compgeo

Research Paper

Effect of anisotropic base/interlayer on the mechanistic responses of layered pavements

Yingchun Cai [a], Ali Sangghaleh [b], Ernian Pan [b,*]

[a] School of Water Conservancy and Environmental Engineering, Zhengzhou University, Zhengzhou, Henan, China
[b] Department of Civil Engineering, University of Akron, Akron, OH, USA

ARTICLE INFO

Article history:
Received 13 June 2014
Received in revised form 12 December 2014
Accepted 21 December 2014

Keywords:
Anisotropy
Interlayer
Layered pavement
Propagator matrix method
MultiSmart3D

ABSTRACT

Material anisotropy and thin interlayer are very common in layered pavement structures. Despite many numerical approaches in pavement analysis, very few theoretical methods are available in dealing with these two important issues. Thus, this study is focused on the effect of anisotropy and thin interlayer on the mechanistic responses of layered pavements. This is done using our analytical solutions based on the propagator matrix method in terms of the cylindrical system of vector functions. Our numerical results show that both anisotropy and thin interlayer could substantially contribute to the pavement responses.

1. Introduction

Layered elastic theory is a powerful method in the mechanistic analysis of layered pavement structures. This theory has always been under constant extension in pavement engineering to make it more appropriate for real pavement conditions [15]. Current works on pavement structures cover a wide range of layered elastic theory generalization including anisotropy, nonlinear elasticity, plasticity, viscoelasticity, and imperfect bonding. One of the notable factors which will affect pavement responses is the anisotropic property of the pavement materials [7]. Mechanical behaviors of structures can be much different for anisotropic materials as compared to the isotropic ones. Several studies showed that pavements made of unbound aggregate base and subbase layers exhibit anisotropic properties [34,5,52]. Among the materials used for different layers in pavement structures, the unbound aggregate base and subbase play an important role in load distribution where they protect the weak subgrade soil while providing support for the asphalt concrete surface layer. The mechanistic properties of unbound aggregate base affect the stress–strain state in pavement structures and particularly the critical responses such as the tensile strain at the bottom of asphalt layer and the compressive strain at the top of the subgrade [46]. Particular properties of pavement structures including elastic anisotropy of unbound aggregate can be investigated by field measurement and numerical simulation [48]. The anisotropic properties of granular materials were analyzed via laboratory tests by a couple of researchers [3,43,28]. The properties of anisotropic layers in pavements made of unbound aggregate base, subbase, and granular subgrade were also studied in laboratory by Kim et al. [29] and Ashtiani [7]. It was observed experimentally that the vertical elastic modulus and out-of-plane Poisson's ratio were higher than the horizontal elastic modulus and in-plane Poisson's ratio, respectively [44]. Belokas and Kavvadas [8] proposed an anisotropic incremental plasticity constitutive model for structured soil to study the effect of stress history and bonding on the mechanical behavior of cohesive soils. The asphalt mixture layer at the top of the pavement and the soil subgrade material were also shown to be anisotropic [2,16]. Therefore, different layers of pavement structures including the unbound aggregate base, subbase, and granular subgrade behave in general as an elastic anisotropic material, although current experimental procedures need to be improved for accurately measuring the anisotropic properties of pavement materials.

Finite element (FE) method is a common technique to analyze the mechanical response of pavements with anisotropic layers. About two decades ago, a program named GT-PAVE was developed to predict the stresses and strains in the pavement where the granular base layer was modeled as nonlinear as well as linear anisotropic [49]. FE programs such as ABAQUS, ANSYS and ADINA were also applied to predict pavement responses under various

* Corresponding author.
E-mail addresses: yccai@zzu.edu.cn (Y. Cai), as147@zips.uakron.edu (A. Sangghaleh), pan2@uakron.edu (E. Pan).

http://dx.doi.org/10.1016/j.compgeo.2014.12.014
0266-352X/

pavement geometry and loading conditions [42,27]. An FE program with material nonlinear anisotropy was also developed for modeling the pavement response with different constitutive relations [34]. Static and dynamic mechanical responses of pavements with anisotropic layers were evaluated using ABAQUS software [5,52]. The difference of the stress field between an isotropic and anisotropic asphalt layer pavement was illustrated by Wang et al. [53] through both analytical and FE calculations. The anisotropic properties were introduced in the pavement design using CIRCLY [54]. The anisotropic properties of pavement layers were also analyzed using the mechanistic-empirical backcalculation techniques [35]. Despite these numerical approaches on pavement analyses, few truly theoretical methods are available in dealing with anisotropic pavements.

Besides material anisotropy, a thin interlayer is also common in pavement structures [26,32]. The use of geotextile interlayers (nonwoven geotextile in particular) in pavement, as alternative to hot mix asphalt (HMA) between cementitious layers, is proven to improve the efficiency and pavement performance [21]. However, a weak thin interlayer may induce serious distress and fracture in the pavement [33] since the stress distribution there could be significantly influenced by the bonding state at the interface [38]. Tack coats and geotextiles can be used to achieve proper bonding between the pavement layers, with surface macro-texture and precise amount of tack coat being two important factors related to this technology [39]. Recently, Kim et al. [26] developed an experimental approach to characterize the interlayer behavior in asphalt pavements and found that its behavior depended strongly on the temperature.

Furthermore, due to the excellent tensile strength of geotextiles, geosynthetics are also used in asphalt concrete pavements to postpone reflective cracks [25]. The interlayers can prevent the formation and propagation of cracks by relieving thermally induced stresses. The Louisiana Department of Transportation adopted a pavement design where granular materials were added between the soil–cement base and the hot mix asphalt surface layer [47]. The goal is to evaluate the capability of the stone interlayer in reducing reflective cracking in flexible pavements, which could be a challenge as illustrated by Chen et al. [13]. FE analysis was carried out by Budkowska and Yu [10], Saad et al. [40], and Chazallon et al. [12] to investigate the benefits provided by geosynthetic reinforcement to fatigue and rutting resistance of flexible pavement. Budkowska and Yu [10] investigated the mitigation of rutting process by geogrids in flexible pavement structure and further validated the methodology with experimental results. By investigating how the fatigue and rutting strain criteria were influenced by the base quality and thickness as well as the subgrade quality, Saad et al. [40] found that placing the geosynthetic reinforcement at the base-asphalt concrete interface would lead to significant reduction of fatigue strain. We further mention that the bonding fatigue performance between two asphalt concrete layers was investigated by Diakhate et al. [17] and the influence of interlayer contact on the fatigue life of asphalt pavement by Ai et al. [4].

Recently we proposed a theoretical approach based on the theory of layered elasticity and implemented it into the software product *MultiSmart3D* (a forward calculation program to analyze the pavement response designed by the Computer Modeling and Simulation Group at the University of Akron). The vigorous analytical solutions are derived via the propagator matrix method in terms of cylindrical and Cartesian systems of vector functions [14] and have been applied successfully to the analysis of real pavement structures [20,41,11]. In this paper, we extend our solutions to include both the material anisotropy and thin interlayer in pavement responses. As numerical examples, the surface deflection and the interior stress/strain response of the pavement with anisotropic base and thin interlayer are analyzed to demonstrate their important influence on these key pavement response behaviors.

2. Theoretical background

2.1. Transverse isotropy

It is well-known that nearly all materials in nature are of elastic anisotropy. Earth materials, due to the gravitational force, normally show the special transverse isotropy with the vertical z-axis being the material symmetry. Thus, the general form of the constitutive relation between the stress tensor (σ_{ij}) and strain tensor (ε_{ij}) for a transversely isotropic medium can be written in terms of the cylindrical coordinate system (r,θ,z) as

$$
\begin{aligned}
\sigma_{rr} &= c_{11}\varepsilon_{rr} + c_{12}\varepsilon_{\theta\theta} + c_{13}\varepsilon_{zz} \\
\sigma_{\theta\theta} &= c_{12}\varepsilon_{rr} + c_{11}\varepsilon_{\theta\theta} + c_{13}\varepsilon_{zz} \\
\sigma_{zz} &= c_{13}\varepsilon_{rr} + c_{13}\varepsilon_{\theta\theta} + c_{33}\varepsilon_{zz} \\
\sigma_{\theta z} &= 2c_{44}\varepsilon_{\theta z}; \quad \sigma_{rz} = 2c_{44}\varepsilon_{rz}; \quad \sigma_{r\theta} = 2c_{66}\varepsilon_{r\theta}
\end{aligned} \tag{1}
$$

where c_{ij} are the elastic stiffness with $c_{66} = 0.5(c_{11} - c_{12})$. Thus for a transversely isotropic material, there are a total of five independent elastic constants. These five elastic constants can be also expressed in terms of the five engineering coefficients as

$$
\begin{aligned}
c_{11} &= \frac{E_h[1-(E_h/E_v)]\mu_v^2}{(1+\mu_h)[1-\mu_h-(2E_h/E_v)\mu_v^2]} \\
c_{12} &= \frac{E_h[\mu_h+(E_h/E_v)\mu_v^2]}{(1+\mu_h)[1-\mu_h-(2E_h/E_v)\mu_v^2]} \\
c_{13} &= \frac{E_h\mu_v}{1-\mu_h-(2E_h/E_v)\mu_v^2}; \quad c_{33} = \frac{E_v(1-\mu_h)}{1-\mu_h-(2E_h/E_v)\mu_v^2} \\
c_{44} &= G_v \quad c_{66} \equiv \frac{c_{11}-c_{12}}{2} = \frac{E_h}{2(1+\mu_h)}
\end{aligned} \tag{2}
$$

where E_h and E_v are the Young's moduli within the plane of transverse isotropy and normal to it, respectively; μ_h and μ_v are Poisson's ratios characterizing the lateral strain response in the plane of transverse isotropy relative to the in-plane strain and the strain normal to it, respectively; and G_v is the shear modulus in the plane normal to the plane of transverse isotropy.

Since the strain energy should be always positive in the elastic material, all principal minors of the stiffness matrix $[c_{ij}]$ in Eq. (1) must be positive [6,51]. This leads to the following constraints on the five engineering coefficients.

$$
\begin{aligned}
& E_v, E_h, G_v > 0 \\
& -1 < \mu_h < 1 \\
& -\sqrt{\frac{E_v}{E_h}\cdot\frac{1-\mu_h}{2}} < \mu_v < \sqrt{\frac{E_v}{E_h}\cdot\frac{1-\mu_h}{2}}
\end{aligned} \tag{3}
$$

With the constitutive relation in Eq. (1) and the involved coefficients being defined, one can then solve a given boundary value problem by combining the well-known equilibrium equations and strain–displacement equations.

2.2. Solution of a layered elastic system

The FE method and layered elastic theory are the common numerical and analytical methods in mechanistic analysis of layered pavements. Common FE software programs including ANSYS, ABAQUS, and ADINA are currently used widely [27,1]. As for the analytical methods, several computer programs were also developed based on the theory of layered elasticity, including BISAR, KENLAYER, JULEA, LEAF, EVERSTRESS, CHERON, ELESYM5 [18,9,45,23]. While numerical methods including FE could be time-consuming, analytical methods are very popular in pavement engineering due to their efficient and easy operation features.

A vigorous analytical method was introduced by Pan [36,37] based on the propagator matrix method in terms of cylindrical and Cartesian systems of vector functions. In this paper, we extend this method to include thin interlayer and material anisotropy in the pavement structures.

Following Pan [37], in order to analyze the mechanistic response of a layered pavement (in the half space $z > 0$) under loadings within a circular area on the surface $z = 0$, the cylindrical system of vector functions can be conveniently used, which is defined as follows [50].

$$\begin{aligned} \boldsymbol{L}(r,\theta;\lambda,m) &= \boldsymbol{e}_z S(r,\theta;\lambda,m) \\ \boldsymbol{M}(r,\theta;\lambda,m) &= \left(\boldsymbol{e}_r \frac{\partial}{\partial r} + \boldsymbol{e}_\theta \frac{\partial}{r\partial\theta}\right) S(r,\theta;\lambda,m) \\ \boldsymbol{N}(r,\theta;\lambda,m) &= \left(\boldsymbol{e}_r \frac{\partial}{r\partial\theta} - \boldsymbol{e}_\theta \frac{\partial}{\partial r}\right) S(r,\theta;\lambda,m) \end{aligned} \tag{4a}$$

where $\boldsymbol{e}_r$, $\boldsymbol{e}_\theta$, and $\boldsymbol{e}_z$ are the unit vectors along the coordinate axes r, θ, and z, respectively, and

$$S(r,\theta;\lambda,m) = \frac{1}{\sqrt{2\pi}} J_m(\lambda r) e^{im\theta}; \quad m = 0, \pm 1, \pm 2, \ldots \tag{4b}$$

where $J_m(\lambda r)$ is the Bessel function of order m with $m = 0$ corresponding to the axial symmetric deformation; $i = \sqrt{-1}$; λ and m are the transformation variables corresponding to the horizontal physical variables r and θ; and the function S satisfies the Helmholtz equation.

Due to the orthonormal properties of the vector functions in Eq. (4a) [50], a vector function, such as the displacement and traction vectors, at any z-level can be expressed as follows.

$$\begin{aligned} \boldsymbol{u}(r,\theta,z) = \sum_m \int_0^{+\infty} [&U_L(z)\boldsymbol{L}(r,\theta) + U_M(z)\boldsymbol{M}(r,\theta) \\ &+ U_N(z)\boldsymbol{N}(r,\theta)]\lambda d\lambda \end{aligned} \tag{5a}$$

$$\begin{aligned} \boldsymbol{t}(r,\theta,z) &\equiv \sigma_{rz}\boldsymbol{e}_r + \sigma_{\theta z}\boldsymbol{e}_\theta + \sigma_{zz}\boldsymbol{e}_z \\ &= \sum_m \int_0^{+\infty} [T_L(z)\boldsymbol{L}(r,\theta) + T_M(z)\boldsymbol{M}(r,\theta) \\ &\quad + T_N(z)\boldsymbol{N}(r,\theta)]\lambda d\lambda \end{aligned} \tag{5b}$$

where U_L, U_M, U_N, T_L, T_M, and T_N are the expansion coefficients in the systems of vector functions. They are functions of z and (λ, m) and are related to the physical-domain displacement and traction vectors on the left-hand side of Eq. (5) as

$$\begin{aligned} U_L(z) &= \int_0^{2\pi}\int_0^{+\infty} \boldsymbol{u}(r,\theta,z)\cdot\bar{\boldsymbol{L}}(r,\theta) r dr d\theta \\ U_M(z) &= \lambda^{-2}\int_0^{2\pi}\int_0^{+\infty} \boldsymbol{u}(r,\theta,z)\cdot\bar{\boldsymbol{M}}(r,\theta) r dr d\theta \\ U_N(z) &= \lambda^{-2}\int_0^{2\pi}\int_0^{+\infty} \boldsymbol{u}(r,\theta,z)\cdot\bar{\boldsymbol{N}}(r,\theta) r dr d\theta \end{aligned} \tag{6a}$$

$$\begin{aligned} T_L(z) &= \int_0^{2\pi}\int_0^{+\infty} \boldsymbol{t}(r,\theta,z)\cdot\bar{\boldsymbol{L}}(r,\theta) r dr d\theta \\ T_M(z) &= \lambda^{-2}\int_0^{2\pi}\int_0^{+\infty} \boldsymbol{t}(r,\theta,z)\cdot\bar{\boldsymbol{M}}(r,\theta) r dr d\theta \\ T_N(z) &= \lambda^{-2}\int_0^{2\pi}\int_0^{+\infty} \boldsymbol{t}(r,\theta,z)\cdot\bar{\boldsymbol{N}}(r,\theta) r dr d\theta \end{aligned} \tag{6b}$$

where the overbar indicates the complex conjugate and the dot between two vectors denotes dot product of the two vectors.

The in-plane stress components can be obtained using these equations and the constitutive relation in Eq. (1). Making use of Eq. (5) and carrying out some simple mathematical operations, we arrive at the following ordinary differential equations for the expansion coefficients in Eq. (5) [36].

$$\begin{aligned} dU_L/dz &= \lambda^2 U_M c_{13}/c_{33} + T_L/c_{33} \\ dU_M/dz &= -U_L + T_M/c_{44} \\ dT_L/dz &= \lambda^2 T_M \\ dT_M/dz &= \lambda^2 U_M(c_{11}c_{33} - c_{13}^2)/c_{33} - c_{13}T_L/c_{33} \end{aligned} \tag{7a}$$

$$\begin{aligned} dU_N/dz &= T_N/c_{44} \\ dT_N/dz &= \lambda^2 c_{66} U_N \end{aligned} \tag{7b}$$

Since in this paper, we consider only the vertical load in a circular area on the surface, which is axis-symmetric, the solution related to the N-type will be automatically zero, and thus, will not be discussed thereafter. Furthermore, due to axisymmetry, all the solutions should be independent of variable θ. In other words, $\partial f/\partial\theta = 0$ for any physical quantity f and $m = 0$ in Eq. (4) for the involved cylindrical function S.

From Eq. (7a), one can easily find the solution matrix $[\boldsymbol{Z}(z)]$ in each layer and thus the corresponding propagator matrix $[\boldsymbol{a}(z)]$ between two adjacent layers as [36,37]

$$[\boldsymbol{E}(z)] = [\boldsymbol{Z}(z)][\boldsymbol{K}] \tag{8a}$$

$$[\boldsymbol{E}(z_{j-1})] = [\boldsymbol{a}(z_j - z_{j-1})][\boldsymbol{E}(z_j)] \tag{8b}$$

where $[\boldsymbol{E}(z)]$ is the expansion coefficient column matrix defined by

$$[\boldsymbol{E}(z)] = [U_L(z), \lambda U_M(z), T_L(z)/\lambda, T_M(z)]^T \tag{9}$$

and $[\boldsymbol{K}]$ is a 4×1 column coefficient matrix with its elements to be determined by the continuity and/or boundary conditions. Also in Eq. (8b), z_{j-1} and z_j are, respectively, the z-level coordinates of the upper and lower interfaces of layer j (Fig. 1). It is also noticed that Eq. (8b) can be propagated from one layer to the other repeatedly so that the unknown coefficients $[\boldsymbol{K}]$ in Eq. (8a) can be connected to the boundary conditions on the surface of the layered pavement and to be solved. This is presented below briefly.

We assume that there is a vertical load uniformly applied over a circular area ($r < R$) on the surface of the layered pavement with density q, as shown in Fig. 1. The layered pavement is made of n layers over a homogeneous half space with the bottom interface of layer j at $z = z_j$. Each layer can be transversely isotropic with five independent elastic coefficients E_h, E_v, μ_h, μ_v, and G_v.

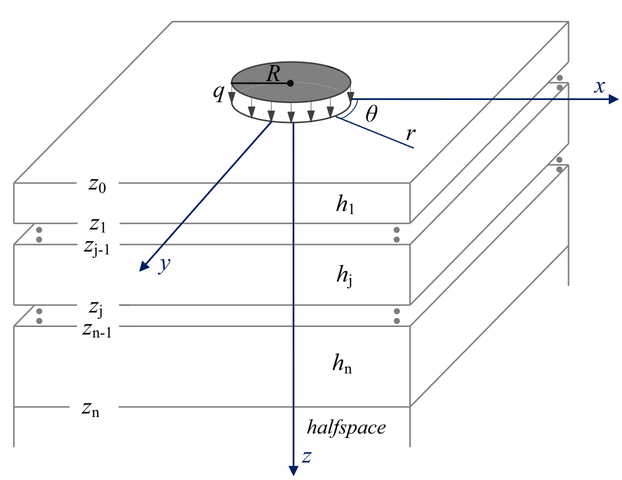

Fig. 1. Circular loading on the surface of a multilayered pavement system.

The boundary conditions on the surface of the layered pavement can be expressed as (for a vertical load of density q within the circle $r = R$ on the surface $z = 0$)

$$\sigma_{zz} = \begin{cases} -q & 0 \leqslant r \leqslant R \\ 0 & r > R \end{cases} \qquad (10)$$
$$\sigma_{rz} = \sigma_{\theta z} = 0$$

Thus, the expansion coefficients for the traction vector on the surface in Eq. (5b) can be found as.

$$T_L(\lambda;0) = \frac{1}{\sqrt{2\pi}}\int_0^{2\pi}\int_0^R -qJ_0(\lambda r)rdrd\theta = -\sqrt{2\pi}RJ_1(R\lambda)q/\lambda \qquad (11)$$
$$T_M(\lambda;0) = T_N(\lambda;0) = 0$$

We now use Eq. (8a) for the homogeneous solution in the half-space (i.e., the last halfspace layer $n + 1$) and the propagating matrix relation in Eq. (8b) to propagate the solution from the bottom of the layered pavement ($z = z_n$) to the surface ($z = z_0 = 0$) to find

$$[\boldsymbol{E}(z_0)] = [\boldsymbol{a}(z_1 - z_0)][\boldsymbol{a}(z_2 - z_1)]\cdots[\boldsymbol{a}(z_n - z_{n-1})][\boldsymbol{Z}(z_n)][\boldsymbol{K}] \qquad (12)$$

In the last halfspace layer, the solution has to be zero at infinity so that two of the corresponding coefficients in $[\boldsymbol{K}]$ have to be zero. On the other hand, on the surface of the layered pavement ($z = 0$), the coefficients T_L and T_M in $[\boldsymbol{E}(z_0)]$ are given by Eq. (11). Therefore, there are four conditions in Eq. (12) which can be used to solve the involved four unknowns (U_L, U_M, and the two coefficients in $[\boldsymbol{K}]$).

After solving the four unknowns involved in Eq. (12), the propagator relation (8b) can be propagated to any z-level to find the expansion coefficients there. Thus, the solutions in terms of the cylindrical system of vector functions can be found at any z-level. With these expansion coefficients, the physical-domain solutions can be obtained by carrying out the inverse transform. In other words, for the described layered pavement under the given vertical surface load over a circle (Eq. (10)) we have the induced displacements and stresses as below [36,14].

$$u_r = \int_0^{+\infty} U_M \frac{\partial S}{\partial r}\lambda d\lambda$$
$$u_\theta = 0 \qquad (13)$$
$$u_z = \int_0^{+\infty} U_L S\lambda d\lambda$$

$$\sigma_{rr} = \int_0^{+\infty}\left[c_{11}U_M\frac{\partial^2 S}{\partial r^2} + c_{12}U_M\frac{\partial S}{r\partial r} + c_{13}\frac{dU_L}{dz}S\right]\lambda d\lambda$$
$$\sigma_{\theta\theta} = \int_0^{+\infty}\left[c_{12}U_M\frac{\partial^2 S}{\partial r^2} + c_{11}U_M\frac{\partial S}{r\partial r} + c_{13}\frac{dU_L}{dz}S\right]\lambda d\lambda$$
$$\sigma_{zz} = \int_0^{+\infty}\left[c_{13}U_M\frac{\partial^2 S}{\partial r^2} + c_{13}U_M\frac{\partial S}{r\partial r} + c_{33}\frac{dU_L}{dz}S\right]\lambda d\lambda \qquad (14)$$
$$\sigma_{\theta z} = 0$$
$$\sigma_{rz} = \int_0^{+\infty}\left[c_{44}\left(\frac{dU_M}{dz}\frac{\partial S}{\partial r} + U_L\frac{\partial S}{\partial r}\right)\right]\lambda d\lambda$$
$$\sigma_{r\theta} = 0$$

The involved integration can be carried out numerically as in Pan [36] and Maina and Matsui [30].

3. Results and discussion

We have checked our formulations for a typical three-layer flexible pavement in Ozawa et al. [35] with an anisotropic base layer (with a vertical to horizontal elastic modulus ratio of 0.5). The first and third layers were assumed to be isotropic and the surface deflections were determined at positions corresponding to the falling weight deflectometer (FWD) sensors positions relative to the center of the loading plate. Vertical circular loading at the top of the pavement surface was 49 kN (the total force applied on the top of the plate) with the plate radius R = 150 mm and with the pavement model similar to Fig. 2. Ozawa et al. [35] calculated the surface deflections using the CRANES software while our results are based on the analytical solutions presented in this paper, as listed in Table 1. It can be observed in Table 1 that the deflection on the surface based on our analytical model agrees well with those obtained by Ozawa et al. [35] based on the software product CRANES. There is a good agreement for surface deflections at different distances from the load center with the maximum relative error being 3% in the third sensor location at 300 mm.

As the first numerical example, we consider a typical three-layer pavement under vertical surface load, with the base layer being anisotropic as shown in Fig. 2. The thickness of each layer is fixed, and the first and third layers are assumed to be isotropic with fixed elastic moduli and Poisson's ratios as listed in Fig. 2. The circular vertical load density on the surface equals q = 700 kPa with a plate radius R = 150 mm.

In order to analyze the effect of the unbound aggregate or granular base material anisotropy on the pavement mechanical response, four different vertical elastic moduli (E_v) are considered, relative to the corresponding fixed horizontal modulus (E_h), with ratios 0.5, 1, 3, and 5. The variation of the surface deflections away from the loading center is calculated for this layered pavement and is shown in Fig. 3 for different moduli ratios (E_v/E_h). It is clearly observed that, for a fixed moduli ratio, the surface deflection (magnitude) decreases with increasing distance from the load center, and that, for fixed observation point (or sensor location), the magnitude of the deflection increases with decreasing moduli ratio.

The variations of strains at critical depths versus horizontal distance are shown in Figs. 4 and 5 for different moduli ratios. It is observed from Fig. 4 that, directly under the loading center, the horizontal strain at the bottom of the asphalt concrete can be affected by the moduli ratio in the base layer. A decrease in the moduli ratio to 0.5 (compared to the isotropic case with a ratio 1) could increase the horizontal strain about 1.3 times (from 0.018% to 0.024%), thus this increase could initiate fatigue cracks there and then propagate to the surface of asphalt concrete to damage the pavement [24].

The variation of the vertical strain on the top and bottom of the base layer is shown, respectively, in Fig. 5a and b. It is observed that near the loading center and on these two depths, the moduli ratio (or material anisotropy) can significantly influence the vertical strain, which should be considered in the pavement design. The results are in agreement with Steyn et al. [46] in which the

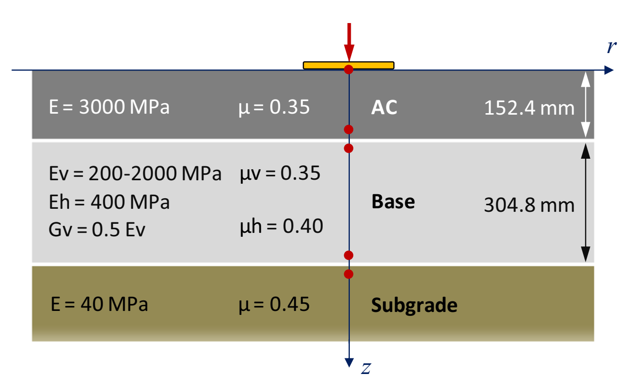

Fig. 2. Schematic diagram of a typical flexible pavement with an anisotropic base layer.

Table 1
Comparison of surface deflections (u_z) at nine sensor locations on the layered pavement as described by Ozawa et al. [35].

Distance r (mm)	0	200	300	450	600	900	1200	1500	2000
Surface deflection u_z (mm) [35]	0.49	0.43	0.39	0.35	0.31	0.24	0.19	0.16	0.12
Surface deflection u_z (mm) (present study)	0.501	0.441	0.402	0.351	0.309	0.243	0.195	0.160	0.118
Relative error (%)	2.2	2.5	3.0	0.3	0.5	1.3	2.9	0.2	1.3

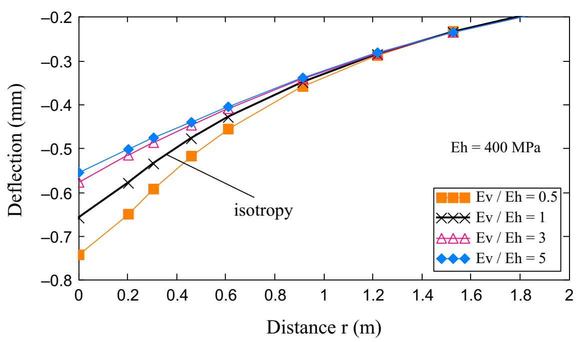

Fig. 3. Variation of deflection (u_z) on the surface vs. horizontal distance (r) for different ratios of vertical to horizontal moduli (E_v/E_h) in the anisotropic base layer.

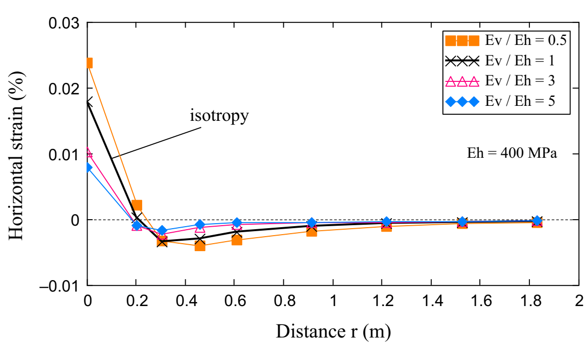

Fig. 4. Variation of horizontal strain (ε_{rr}) vs. horizontal distance (r) at the bottom of asphalt concrete layer ($z = 150$ mm) for different ratios of vertical to horizontal moduli (E_v/E_h) in the anisotropic base layer.

anisotropy has more profound effect on the mechanistic behavior of the base layer than on the asphalt concrete layer. Our calculation indicates that different moduli ratios will also affect the vertical strain at the top of the subgrade layer, particularly directly below the loading center. This will contribute to and influence the rutting life prediction as discussed below.

It is important to mention that the strain variations (Figs. 4 and 5) in the pavement with anisotropic base layer are obtained by assuming a fixed horizontal modulus in the base layer. While we have shown clearly that the pavement response depends significantly on the anisotropy of the base layer, we show next that the actual modulus value of the base layer will also remarkably contribute to the pavement response. The deflections at the surface and strains at the center ($r = 0$) and at critical z-levels in the pavement for three different values of the base horizontal modulus are illustrated in Fig. 6. For a fixed moduli ratio, the magnitude of the surface deflection (Fig. 6a), the horizontal strain at the bottom of asphalt, and the magnitude of the vertical strain at the top of the subgrade (Fig. 6b) all decrease with increasing horizontal modulus E_h. The magnitude of the surface deflection and the horizontal strain at the bottom of asphalt will decrease with increasing moduli ratio (E_v/E_h) at all three horizontal moduli. However, the magnitude of the vertical strain at the top of the subgrade (Fig. 6b) will increase with increasing moduli ratio (E_v/E_h).

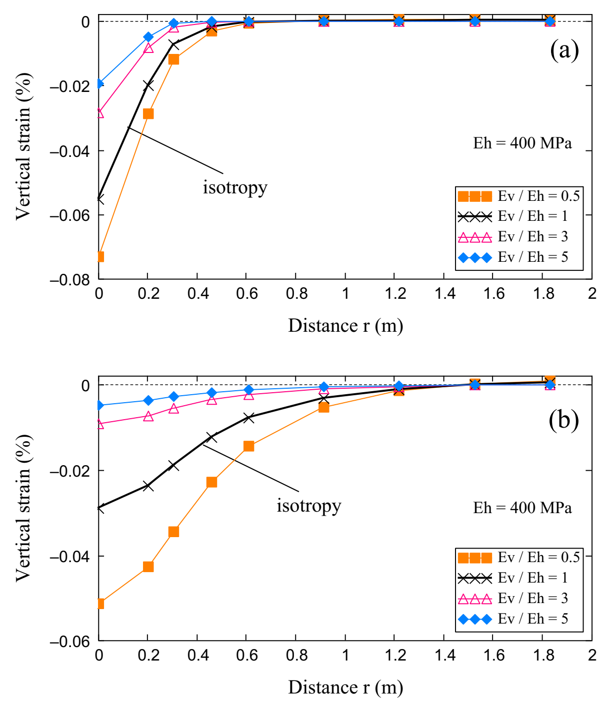

Fig. 5. Variation of vertical strain (ε_{zz}) at the top of base layer ($z = 155$ mm) in (a) and of vertical strain (ε_{zz}) at the bottom of base layer ($z = 455$ mm) in (b) vs. horizontal distance (r) for different ratios of vertical to horizontal moduli (E_v/E_h) in the anisotropic base layer.

Strains at the bottom of the asphalt concrete and the top of the subgrade are critical for the prediction of the fatigue and rutting life of the pavement structures. As an example, we now apply our strain results to the fatigue model as described in FHWA [19] and the Shell rutting model as presented by Gonçalves et al. [22] to investigate the effect of material anisotropy on the pavement life. The fatigue design life for a flexible pavement with hot rolled asphalt layer at temperature 20 °C could be calculated using the following relationship [19]

$$N_f = (1.660 \times 10^{-10})(1/\varepsilon_r)^{4.32} \tag{15}$$

where N_f is the predicted life in standard axles and ε_r ($\equiv \varepsilon_{rr}$) is the horizontal tensile strain at the bottom of the asphalt layer under a standard wheel load. The rutting design life for a flexible pavement is as follows [22].

$$N_r = f_1(\varepsilon_v)^{-f_2} \tag{16}$$

where N_r is the number of allowed road repetitions and ε_v ($\equiv \varepsilon_{zz}$) is the vertical compressive strain at the top of the subgrade. The model parameters f_1 and f_2 are available for different corporation designs [22]. We consider the Shell model parameters with $f_1 = 6.150 \times 10^{-7}$ and $f_2 = 4$, respectively.

Fig. 7 shows the number of life cycles versus the moduli ratio in the pavement. It can be observed that, when the moduli ratio is less than 1 ($E_v/E_h < 1$) and when it decreases, the fatigue life of the pavement decreases but the rutting life increases. On the contrary, when the moduli ratio is larger than 1 ($E_v/E_h > 1$) and when it

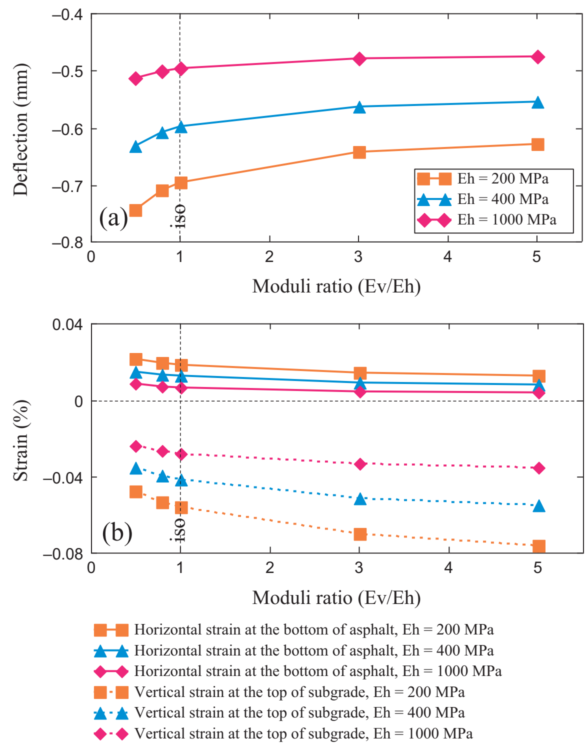

Fig. 6. Deflection (u_z) at the origin $(r,\theta,z) = (0,0,0)$ on the surface in (a) and horizontal and vertical strains (ε_{rr} and ε_{zz}) at critical z-levels in (b) in the pavement structure vs. moduli ratio (E_v/E_h) in the anisotropic base layer.

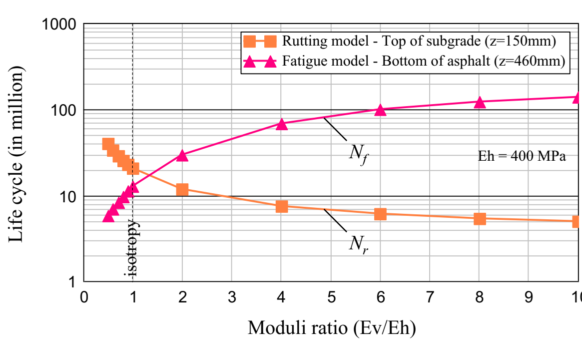

Fig. 7. Life prediction of the pavement structure with an anisotropic base layer as shown in Fig. 2 based on the FHWA [19] fatigue model (N_f in Eq. (15)) and the Shell rutting model (N_r in Eq. (16)) [22].

increases, the fatigue life will increase but the rutting life will decrease.

In the second numerical example, our layered pavement contains a thin anisotropic interlayer (between the asphalt concrete and base layers) with material properties and geometry shown in Fig. 8. The interlayer behaves similar to the geotextile reinforcement with material anisotropy. A load density of $q = 700$ kPa is applied on the surface of the pavement within a circular area of radius $R = 150$ mm. For fixed interlayer thickness, different moduli ratios of the interlayer (vertical modulus over horizontal modulus) are assumed to study their effect on the pavement response. Shown in Fig. 9 is the deflection on the surface of the pavement with intervals equivalent to the sensor locations in standard FWD tests. It is noted that, in general, away from the loading area, the effect of the moduli ratio could be neglected; only for the very severe case where the ratio is reduced to 0.001, one can observe the obvious effect of anisotropy on the surface deflection near

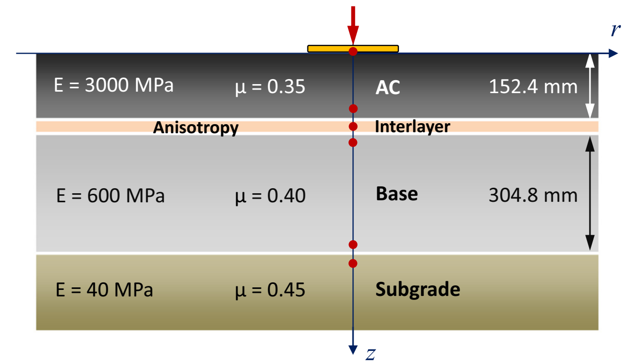

Fig. 8. Schematic diagram of a pavement containing an anisotropic thin interlayer between the asphalt concrete and base layers (Thickness of the interlayer is 5 mm and the material properties are $E_h = 4000$ MPa, $\mu_h = 0.25$, $E_v = 4$–4000 MPa, $\mu_v = 0.01$, and $G_v = 1600$ MPa).

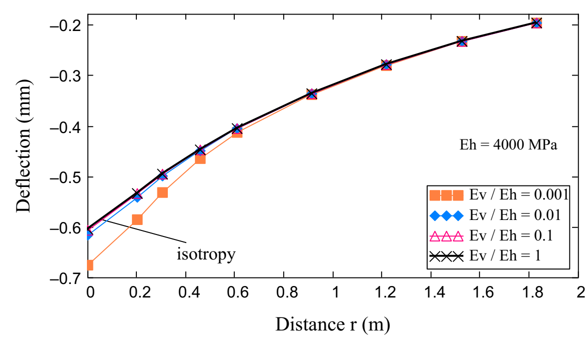

Fig. 9. Variation of deflection (u_z) on the surface vs. horizontal distance (r) for different vertical to horizontal moduli ratios (E_v/E_h) in the interlayer.

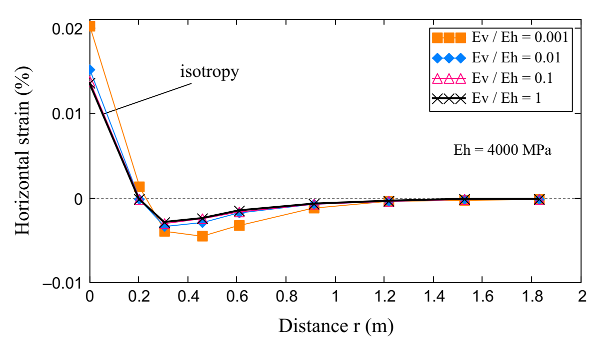

Fig. 10. Variation of horizontal strain (ε_{rr}) at the bottom of asphalt concrete layer ($z = 150$ mm) vs. horizontal distance (r) for different vertical to horizontal moduli ratios (E_v/E_h) in the interlayer.

the loading area. Similarly, the effect of the moduli ratio on the horizontal strain at the bottom of asphalt layer is also very small as shown in Fig. 10. Fig. 11 shows the vertical strain in the middle of the interlayer for different moduli ratios. It can be observed that the vertical strain can be significantly affected by the moduli ratio, particularly directly below the loading area. The horizontal and vertical strains at the bottom of the base layer and the vertical strain at the top of the subgrade layer are shown, respectively, in Figs. 12a and b and 13 for different moduli ratios. It can be seen that the strain field can be significantly affected when the ratio of the vertical to horizontal modulus becomes small. The horizontal strain is positive (tensile) below the applied load and at the bottom of base layer. Away from the loading center, the horizontal strain becomes negative (compressive) and approaches zero with

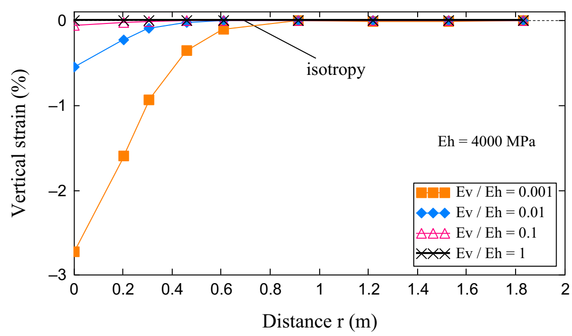

Fig. 11. Variation of vertical strain (ε_{zz}) in the middle of interlayer ($z = 154.9$ mm) vs. horizontal distance (r) for different vertical to horizontal moduli ratios (E_v/E_h) in the interlayer.

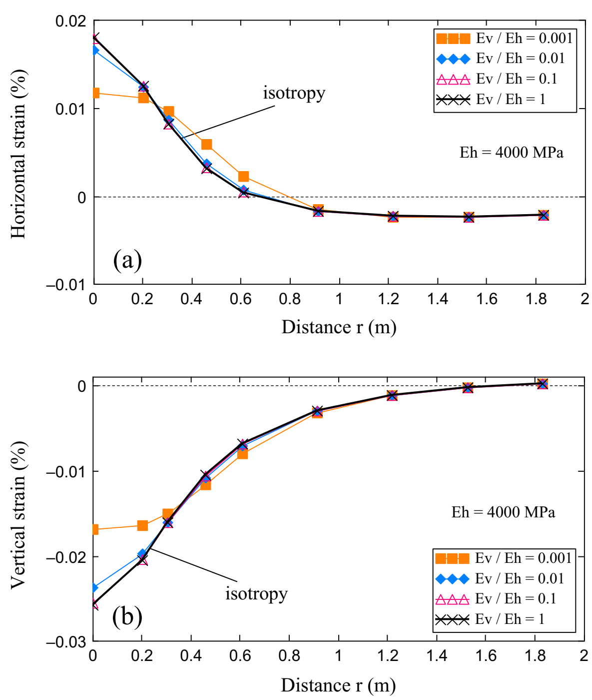

Fig. 12. Variation of horizontal strain (ε_{rr}) in (a) and vertical strain (ε_{zz}) in (b) at the bottom of base layer ($z = 460$ mm) vs. horizontal distance (r) for different vertical to horizontal moduli ratios (E_v/E_h) in the interlayer.

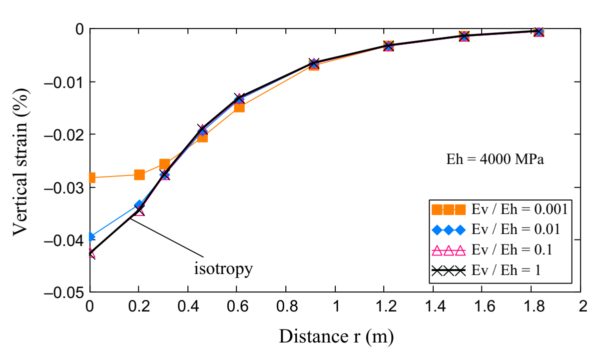

Fig. 13. Variation of vertical strain (ε_{zz}) at the top of subgrade layer ($z = 465$ mm) vs. horizontal distance (r) for different vertical to horizontal moduli ratios (E_v/E_h) in the interlayer.

increasing distance away from the loading center (Fig. 12a). In contrast, the vertical strain at both sides of the base-subgrade interface is always negative and approaches zero far away from the loading center (Figs. 12b and 13). These results demonstrate the importance of the critical strains (and the corresponding state of stress) in terms of the fatigue and rutting life prediction which is useful for pavement design, rehabilitation, and maintenance. We point out that a relatively thin layer in layered structures could be efficiently represented by a modified imperfect interface condition on the displacements and tractions, as discussed and reviewed by Martin [31].

A construction method for a pavement can only be trusted if it originates from a very well designed procedure supported by theoretical analysis. In the current mechanistic-empirical pavement design guide, a wide variety of materials are considered for different layers and these materials are only recognized by isotropic elastic modulus and Poisson's ratio. The current design could be modified to include all five transversely isotropic elastic moduli for more accurate deflection and strain calculations. Thus, our analytical technique could be incorporated into the design procedure in the way that the displacement and stress/strain can be easily calculated at critical locations in the pavement with material anisotropy to further reinforce and modify the models for overlay design as well as fatigue and rutting predictions in pavement structures.

4. Conclusions

Based on the cylindrical system of vector functions and making use of the propagator matrix method, we have presented an analytical method to accurately predict the responses of a layered pavement with thin interlayer and material anisotropy. The displacement, strain, and stress fields can be precisely calculated for a field point at any location in the layered pavement. Two typical layered pavement models are presented. Numerical results show that the deflection on the surface and the strain at the critical locations in the pavement could be significantly affected by the material anisotropy and thin interlayer. More specifically, for the pavement with an anisotropic base layer, the deflection at the surface, the horizontal strain at the bottom of the asphalt concrete layer, and the vertical strain in the base layer can be greatly affected by the anisotropy of unbound granular base. For the pavement with an anisotropic thin interlayer of thickness 5 mm, it is found that the deflection on the surface, the horizontal strain at the bottom of asphalt concrete layer, the vertical and horizontal strains at the bottom of the base layer, and the vertical strain at the top of subgrade would be also remarkably influenced by the horizontal to vertical moduli ratio of the thin interlayer. Thus, our numerical examples clearly demonstrate that, in general, the response of a layered pavement is obviously affected by the material anisotropy and/or thin interlayer. Consequently, the design life of a layered pavement could be also significantly influenced by the pavement anisotropy and thin interlayer.

Acknowledgement

The first author (Y.C. Cai) would like to thank the University of Akron for providing a visiting professor position to carry out this research work.

References

[1] Abed AH, Al-Azzawi AA. Evaluation of rutting depth in flexible pavements by using finite element analysis and local empirical model. Am J Eng Appl Sci 2012;5(2):163–9.
[2] Abelev AV, Lade PV. Characterization of failure in cross-anisotropic soils. J Eng Mech 2004;130(5):599–606.
[3] Adu-Osei A. Characterization of unbound granular layers in flexible pavements. PhD thesis. College Station (TX): Texas A&M Univ.; 2000.

[4] Ai C, Cheng M, Yang T, Qiu Y. Bending fatigue test and interlayer pavement models for beams of asphalt mixture. J Highway Transport Res Develop 2012;6(4):23–7.
[5] Al-Qadi IL, Wang H, Tutumluer E. Dynamic analysis of thin asphalt pavements by using cross-anisotropic stress–dependent properties for granular layer. Transportation Research Board, No. 2154, Transportation Research Board of the National Academies, Washington (DC); 2010. p. 156–163.
[6] Amadei B, Pan E. Gravitational stresses in anisotropic rock masses with inclined strata. Int J Rock Mech Min Sci 1992;29(3):225–36.
[7] Ashtiani RS. Anisotropic characterization and performance prediction of chemically and hydraulically bounded pavement foundations. PhD thesis. Texas: Texas A&M University; 2009.
[8] Belokas G, Kavvadas M. An anisotropic model for structured soils Part I: Theory. Comput Geotech 2010;37:737–47.
[9] BISAR. Shell pavement design methodology. The Netherlands: Shell Petroleum Company; 1989.
[10] Budkowska BB, Yu J. Mitigation of short term rutting by interlocking layer developed around a geogrids-sensitivity analysis. Comput Geotech 2003;30:61–79.
[11] Cai YC, Pan E, Sangghaleh A. Inverse calculation of elastic moduli in cross-anisotropic and layered pavements by system identification method. Inverse Probl Sci Eng 2014. http://dx.doi.org/10.1080/17415977.2014.933833.
[12] Chazallon C, Koval G, Hornych P, Allou F, Mouhoubi S. Modelling of rutting of two flexible pavements with the shakedown theory and the finite element method. Comput Geotech 2009;36:798–809.
[13] Chen Y, Lopp G, Roque R. Effects of asphalt rubber membrane interlayer (ARMI) on pavement reflective cracking performance. J Mater Civ Eng 2013. http://dx.doi.org/10.1061/(ASCE)MT.1943-5533.0000781.
[14] Chen YG, Pan E. Responses of transversely isotropic layered half-space to multiple horizontal loads. In: You Z, Abbas AR, Wang L, editors. ASCE geotechnical special publication no. 182. Pavements and materials: characterization, modeling and simulation; 2008. p. 63–77.
[15] Coleri E, Harvey JT. Investigation of layered elastic theory prediction accuracy for asphalt concrete pavement design using micromechanical viscoelastic finite element modeling. Mater Des 2014;47(3):411–32.
[16] De Melo L, Cabral BP. Inherent anisotropy in pavement subgrades. ASCE Geo Congr 2012:1056–65.
[17] Diakhate M, Millien A, Petit C, Phelipot-Mardele A, Pouteau B. Experimental investigation of tack coat fatigue performance: towards an improved lifetime assessment of pavement structure interfaces. Constr Build Mater 2011;25:1123–33.
[18] FHWA. ELSYM5 interactive microcomputer version. Report FHWA-TS-87-217, Federal Highway Administration. Washington (DC); 1987.
[19] FHWA. Fatigue performance of IDOT mixtures. Report FHWA-ICT-007-2007, Federal Highway Administration, Washington (DC); 2006.
[20] FHWA. An efficient and accurate genetic algorithm for backcalculation of flexible pavement layer moduli. Report FHWA/OH-2012/18, Federal Highway Administration, Washington (DC); 2012.
[21] Garber S, Rasmussen RO. Nonwoven geotextile interlayers in concrete pavements. Transportation Research Record, Journal of the Transportation Research Board, No. 2152, Washington (DC); 2010. p. 11–15.
[22] Gonçalves FP, Ceratti A, Bernucci E. Study of permanent deformations in asphalt concrete layers. In: Collop, Brown, editors. Performance of bituminous and hydraulic materials in pavements. Swets & Zeitlinger, Lisse; 2002. p. 73–8.
[23] Hayhoe GF. LEAF: a new layered elastic computational program for federal aviation administration pavement design and evaluation procedures. In: Federal aviation administration, airport technology transfer conference. Atlantic City (NJ); 2002.
[24] Hu X, Walubita LF. Modelling tensile strain response in asphalt pavements bottom-up and/or top-down fatigue crack initiation. Road Mater Pavement Des Int J 2009;10:125–54.
[25] Khodaii A, Fallah Sh. Effects of geosynthetic reinforcement on the propagation of reflection cracking in asphalt overlays. Int J Civ Eng 2009;7(2):131–40.
[26] Kim H, Arraigada M, Raab C, Partl MN. Numerical and experimental analysis for the interlayer behavior of double-layered asphalt pavement specimens. J Mater Civ Eng 2011;23(1):12–20.
[27] Kim M, Tutumluer E, Kwon J. Nonlinear pavement foundation modeling for three-dimensional finite-element analysis of flexible pavements. Int J Geomech 2009;9(5):195–208.
[28] Kim SH. Determination of aggregate physical properties and its effect on cross-anisotropic behavior of unbound aggregate materials. PhD thesis. Texas: Texas A&M University; 2004.
[29] Kim SH, Little DN, Masad E, Lytton RL. Estimation of level of anisotropy in unbound granular layers considering aggregate physical properties. Int J Pavement Eng 2005;6(4):217–27.
[30] Maina J, Matsui K. Elastic multi-layered analysis using DE-integration. Res Inst Math Sci 2005;41:853–67.
[31] Martin PA. Boundary integral equations for the scattering of elastic waves by elastic inclusions with thin interface layers. J Nondestr Eval 1992;11:167–74.
[32] Mohammad LN, Hassan M, Patel N. Effects of shear bond characteristics of tack coats on pavement performance at the interface. Transportation Research Record 2209, Transportation Research Board of the National Academies, Washington (DC); 2011. p. 1–8.
[33] Netterberg F, de Beer M. Weak interlayers inflexible and semi-flexible road pavements. J S Afr Inst Civ Eng 2012;54(1):32–42.
[34] Oh JH, Lytton RL, Fernando EG. Modeling of pavement response using nonlinear cross-anisotropy approach. J Transport Eng 2006;132:458–68.
[35] Ozawa Y, Maina J, Matsui K. Influence of cross-anisotropy material behavior on back-calculation analysis of multi-layered systems. In: 6th International conference on road and airfield pavement technology. Sapporo, Japan; 2008.
[36] Pan E. Static response of a transversely isotropic and layered half space to general surface loads. Phys Earth Planet Inter 1989;54:353–63.
[37] Pan E. Static Green's functions in multilayered half-spaces. Appl Math Model 1997;21(8):509–21.
[38] Raab C, Partl MN. Investigation on long-term interlayer bonding of asphalt pavements. Baltic J Road Bridge Eng 2008;3(2):65–70.
[39] Raposeiras AC, Vega-Zamaniloo A, Calzada-Perez MA, Castro-Fresno D. New procedure to control the tack coat applied between bituminous pavement layers. Constr Build Mater 2013;44:228–35.
[40] Saad B, Mitri H, Poorooshasb H. 3D FE analysis of flexible pavement with geosynthetic reinforcement. J Transport Eng 2006;132:402–15.
[41] Sangghaleh A, Pan E, Green R, Wang R, Liu X, Cai Y. Backcalculation of pavement layer elastic modulus and thickness with measurement errors. Int J Pavement Eng 2014;15(6):521–31.
[42] Schwartz CW. Effect of stress–dependent base layer on the superposition of flexible pavement solutions. Int J Geomech 2002;2(3):331–52.
[43] Seyhan U, Tutumluer E. Anisotropic modular ratios as unbound aggregate performance indicators. J Mater Civ Eng 2002;14(5):409–16.
[44] Seyhan U, Tutumluer E, Yesilyurt H. Anisotropic aggregate base inputs for mechanistic pavement analysis considering effects of moving wheel loads. J Mater Civ Eng 2005;17(5):505–12.
[45] Sivaneswaran N, Pierce LM, Mahoney JP. Everstress version 5.0: layered elastic analysis program. Olympia (WA): Washington State Department of Transportation; 2001.
[46] Steyn W, Maina J, Repsold A. Comparison of isotropic and cross-anisotropic analysis of pavement structures. In: Annual meeting of the transportation research board. Washington (DC); 2013.
[47] Titi H, Rasoulian M, Martinez M, Becnel B, Keel G. Long-term performance of stone interlayer pavement. J Transport Eng 2003;129:118–26.
[48] Tutumluer E, Adu-Osei A, Little DN, Lytton RL. Field validation of the cross-anisotropic behavior of unbound aggregate bases. Report ICAR-502-2; 2001.
[49] Tutumluer T. Predicting behavior of flexible pavements with granular bases. PhD thesis. Atlanta (GA): Georgia Institute of Technology; 1995.
[50] Ulitko AF. Method of special vector functions in three-dimensional elasticity. Naukova Dumka, Kiev; 1979. 264p [in Russian].
[51] Wang CD. Displacements and stresses due to vertical subsurface loading for a cross-anisotropic half-space. Soils Found 2003;43(5):41–52.
[52] Wang H, Al-Qadi IL. Importance of nonlinear anisotropic modeling of granular base for predicting maximum viscoelastic pavement responses under moving vehicular loading. J Eng Mech 2013;139(1):29–38.
[53] Wang L, Hoyos LR, Wang J, Voyiadjis G, Abadie C. Anisotropic properties of asphalt concrete: characterization and implications for pavement design and analysis. J Mater Civ Eng 2005;17(5):535–43.
[54] Wardle L. CIRCLY and mechanistic pavement design: the past, present and towards the future. <http://www.mincad.com.au/circlypap.htm>; 2010 [21.04.13].